Dalton Transactions

Accepted Manuscript

ROYAL SOCIETY OF CHEMISTRY

www.rsc.org/dalton

Cite this: DOI: 10.1039/c0xx00000x

www.rsc.org/xxxxxx

ARTICLE TYPE

Polymethyl methacrylate (PMMA) –Bismuth Ferrite (BFO) nanocomposite: Low loss and high dielectric constant materials with perceptible magnetic properties

Mohaseen S. Tamboli,[a] Prakash K. Palei,[a] Santosh S. Patil,[a] Milind V. Kulkarni, [a] Noormahmad. N. Maldar [b] and Bharat B. Kale [a]*

Received (in XXX, XXX) Xth XXXXXXXXX 20XX, Accepted Xth XXXXXXXXX 20XX
DOI: 10.1039/b000000x

Herein, Poly (methyl methacrylate)-Bismuth ferrite (PMMA-BFO) nanocomposites were successfully prepared by in-situ polymerization method for the first time. Initially, the as prepared bismuth ferrite (BFO) nanoparticles were dispersed in the monomer, (methyl methacrylate) using sonication process. Benzoyl peroxide was used to initiate the polymerization reaction in ethyl acetate medium. The nanocomposite films were subjected to X-ray diffraction (XRD), ^{1}H NMR, Field emission scanning electron microscopy (FESEM), Transmission electron microscopy (TEM), Atomic force microscopy (AFM), Thermogravimetric analysis (TGA), Infrared spectroscopy (IR), Dielectric and Magnetic characterizations. The dielectric measurement of the nanocomposites was investigated from 10 Hz to 1 MHz frequency range. It was found that the nanocomposites not only showed a significantly increased value of dielectric constant with increase in loading percentage of BFO as compared to pure PMMA, but also exhibited low dielectric loss values in a wide range of frequencies. The value of dielectric constant and dielectric loss of the PMMA-BFO5 (5% BFO loading) sample at 1 kHz frequency was found be ~ 14 and 0.037. The variation of the ferromagnetic response of the nanocomposite was consistent with the varying volume percentage of the nanoparticles. The remnant magnetization (Mr) and saturation magnetization (Ms) values of the composites were found to be enhanced by increasing the loading percentage of BFO. The value of Ms for PMMA-BFO5 was found to be ~6 emu/g. The prima facie observations suggest that the nanocomposite can be a potential candidate for high dielectric constant capacitors. Significantly, based on its magnetic properties the composite will also be useful for hard disk components.

Introduction

In past few years, high dielectric constant polymer composites have attracted the attention of the researchers, especially in the electronic industries because of its ease of preparation and low cost.[1] An electronic system is comprised of by both active as well as passive components. The technologies which are concerned with the development of the passive components such as resistors, inductors and capacitors are developing, rapidly. Among these passive components, capacitor attracts lots of attention due to its wide range of applications which includes decoupling, by-passing, filtering and timing capacitors etc. In the past several years, significant amount of work has been carried out on various polymer-ceramic composites.[2,3] Among ceramic-polymer composites, special attention has been paid for the development of high dielectric constant ceramic-polymer composites because of its applications mainly in embedded capacitors. These materials have become potential candidates for integration into high frequency electronics. However, the detail understanding of these materials will help the electronic industry in proper planning, design and processing of these materials.

Recent advances in composite field revealed that mainly two primary methods have been used to obtain high dielectric constant in polymer composites. The more traditional one is the addition of high dielectric constant ceramic fillers to the polymer matrix[4-12] and another method is by incorporating conductive fillers into the polymer matrix. In comparison with the research interests in high dielectric constant materials, importance has not been given to the dielectric loss of the material. For many applications including integral thin film capacitors, electrostriction systems for artificial muscles and electric stress control devices, apart from high dielectric constant; low dielectric loss is also required.[13-31] Although, insulating polymers filled with conductive fillers can exhibit high dielectric constants, it possess high dielectric loss values and very low breakdown strengths due to the high electrical conductivity of the fillers, which limits its applications. Recently, high dielectric constant ferroelectric ceramic based polymer nanocomposites have attracted significant interest. These materials generally show relatively low dielectric loss because both the polymer and the ceramic particles are highly insulating in nature.

Ferroelectric ceramics possess very high dielectric constants as well as low dielectric loss. However, these are brittle and suffer mostly because of its low mechanical strength. On the other hand, polymers have low dielectric constants in the range of ~ 2 to 5. Traditionally these polymer nanocomposites are used in low leakage capacitors. Moreover, the flexible nature of polymer nanocomposites make easy processing which results high dielectric strength. Hence, new composites with high dielectric constant and low dielectric loss can be fabricated by combining the properties of both polymers and ceramics. [32-35] In order to achieve such an objective, high dielectric constant ferroelectric ceramics such as $Pb(Mg_{1/3}Nb_{2/3})O_3$- $PbTiO_3$(PMNPT), $Pb(Zr,Ti)O_3$(PZT) and $BaTiO_3$ (BT) have already been used as fillers in polymers. [36-42]

Furthermore, composite materials with reinforcing particles based on permanent magnetic materials like Nd- Fe- based materials are of current research interest due to numerous possible applications, such as hard disc components, electric appliances and automobile industry. In the last several years, the rapid development in the field of electronic processing has led to an increased demand for multifunctional electronic nanocomposites which fulfills the need of electronic devices. [35, 43] In this context, soft magnetic nanoparticles dispersed in polymer matrixes have been extensively studied because of their excellent magnetic as well as electrical properties. [44] Polymer magnetic nanocomposite materials are widely used in various engineering applications like sensor technology, [45] high density storage media, electromagnetic Interference (EMI) suppression, superconductors [46] etc.

Among the multifunctional materials, Bismuth ferrite ($BiFeO_3$) is a well investigated material and is known for its multiferroic properties. It has received considerable interest in the past few years because of having simultaneous ferroelectric and ferromagnetic properties. The multifunctionality property of BFO not only provide opportunities to study fundamental physics but also finds many potential applications in various devices such as information storage, spintronics and sensors. [47-49] Also, it possesses high dielectric constant which is the main concern in this study. However, these nanoparticles need to be embedded in a suitable polymer matrix in order to make it suitable for various applications. Few major problems which arise in case of pure ceramics like high leakage current and dielectric losses, which lead to failure during operation, can also be eliminated in the polymer based composites. Hence, in the present work, we have selected BFO as filler material in the polymer-ceramic composite.

Among the insulating polymers, poly (methyl methacrylate) (PMMA) is a very good insulating polymer. The dielectric constant and dielectric loss of this polymer was reported to be ~ 2.6 and 0.014 at 1MHz frequency respectively. The low dielectric loss of this polymer enables it to be used as a matrix in nanocomposites. In the literature, there is hardly any work which has been devoted to study the electrical, magnetic, structural, vibrational and microstructural properties of the PMMA-BFO nanocomposite. Ahlawat et al. studied the magnetic and dielectric properties of the PMMA-BFO nanocomposites. They found that with the increase in BFO loading in the composite, the magnetic as well as dielectric properties are enhanced. [50] Sun et al reported that with the increase in BFO loading in PMMA, the microwave shielding ability of the composite was increased. [51] However, the properties reported here in this study is not sufficient enough for the device applications. Hence, further study on this nanocomposite is quite necessary.

In the present work, for the first time, we have successfully synthesized the novel PMMA-BFO nanocomposite by *in-situ* chemical polymerization method. The as prepared PMMA-BFO nanocomposites were characterized by various techniques to study its structural, microstructural and vibrational properties. The electrical and magnetic properties of the nanocomposite have also been studied in detail, which is hitherto unattempted. Finally, an effort has also been made to correlate the above properties.

Experimental Section

Materials and Methods

Methyl methacrylate monomer (99% purity,) was stored at low temperature prior to use. Oxidizing agent benzoyl peroxide and ethyl acetate (analytical grade) were used as received. Bismuth nitrate, Ferric nitrate, Nitric acid and Glycine were used as received. All the solutions were prepared using double distilled water during the synthesis.

Synthesis of Bismuth ferrite (BFO)

Bismuth ferrite powder was synthesized by auto combustion method. 0.5 M Bismuth nitrate Bi $(NO_3)_3$ and 0.5 M Ferric nitrate Fe $(NO_3)_3$ solutions were prepared by dissolving in distilled water and small amount of dilute nitric acid. These two solutions were mixed in a beaker. To this solution, Glycine with molar ratio 1:1 with respect to nitrate was added. This solution was then heated on a hot plate under continuous stirring condition to its boiling temperature until all the liquid gets evaporated. Towards the end of the reaction, an immense evolution of brown fumes were observed, a fluffy brown mass was obtained at the base of the beaker. Then the powder was calcined at 500^{o}C for 2 hr and subjected for further characterization.

Synthesis of PMMA-BFO nanocomposite

PMMA-BFO nanocomposite was synthesized by *in-situ* polymerization method. In this method, initially bismuth ferrite nanoparticles (1wt.%) were dispersed in MMA and ethyl acetate, and then ultrasonicated for 30 mins. Finally, the oxidizing agent benzoyl peroxide was added to it with vigorous stirring. The same procedure was followed for the synthesis of PMMA-BFO composites with 3 wt.% and 5 wt. % BFO nanoparticles in the Polymer matrix. The above dispersion was refluxed at 70ºC in water bath with constant stirring over a period of ~10-16 hours to initiate the polymerization of MMA. After completion of the reaction, a gelatinous brownish white solution was obtained. Finally, required amount of methanol was poured to precipitate PMMA-BFO nanocomposite. The nanocomposite was then dissolved in chloroform and cast into film form on the glass slide. This nanocomposite film was then subjected for the various physicochemical characterizations. The samples prepared using 1, 3 and 5% loading are termed as PMMA-BFO1, PMMA-BFO3 and PMMA-BFO5, respectively.

Structural Characterizations

The X-ray diffraction (XRD) studies of the sample were

performed by using X-ray diffractometer (Bruker D8 Advance, Germany). The sample was scanned in the 2θ ranges from 10 to 80°. The field emission scanning electron microscopy (FE-SEM) (Hitachi S-4800 II) was used to determine the morphology of pure BFO and PMMA-BFO nanocomposites. The Transmission electron microscopy (TEM) was performed with (FEI Technai T20 Netherland) an accelerating voltage of 200 kV. AFM images were recorded with a NTEGRA aura model (NT MDT) SPM instrument in semi contact mode using an NSG 01 silicon nitride probe. FTIR spectra BFO, PMMA and PMMA-BFO (1, 3 and 5%) nanocomposite were studied using Perkin-Elmer-Spectrum 2000 spectrophotometer in the range of 400 and 4000 cm^{-1}. Room temperature dielectric properties were measured by Hioki 3532-50 LCR Hitester. The M–H loops were measured at room temperature using a vibration sample magnetometer ~ VSM, model 4500, EG & G Princeton Applied Research Corporation USA.

Results and Discussion

X-ray diffraction (XRD)

Inset of Fig.1 shows the XRD pattern of pure BFO ceramic. Development of single perovskite rhombohedral phase in BFO is confirmed by matching with the JCPDS card no: 71-2494. The unit cell parameters of the BFO ceramics are calculated by X'Pert highscore plus software. The detail parameters are given in Table-1. Fig.1 shows the XRD patterns of PMMA-BFO nanocomposites with different load percentage of BFO nanoparticles. The appearance of a broad peak at 2θ ~ 13° can be attributed to the presence of amorphous polymer chain, while the sharp peaks are the peaks of BFO ceramics. It can be seen that with the increase in loading percentage of BFO nanoparticles, the intensity as well as the sharpness of the peaks are increased, which indicates the increase of crystalline nature of the nanocomposites.

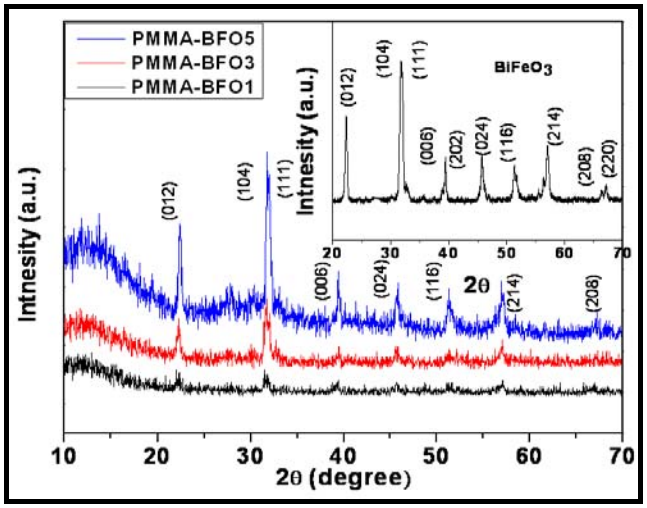

Fig. 1 XRD patterns of PMMA-BFO nanocomposites

Table-1 Structure and unit cell parameters of pure BFO ceramics.

Material	Lattice parameter			Structure	Space group
	a (Å)	b (Å)	c (Å)		
BFO	5.584(3)	5.584(3)	13.86(1)	Rhombohedral	R3C

NMR Spectra

The ^{1}H NMR spectra of the nanocomposites was taken to provide more detail evidence about the growth of BFO nanoparticles in PMMA matrix. As seen from Fig. 2, all the characteristic proton absorption bands associated with PMMA could be clearly detected in the ^{1}H NMR spectrum of PMMA and PMMA-BFO. Table 2 shows the tacticity of pure PMMA[30] and PMMA-BFO nanocomposites. It should be noted that the as synthesized PMMA and PMMA-BFO nanocomposites shows significantly different values of tacticity. It can be clearly seen here that apart from the appearance of distinct proton signals for methoxy ($OCOCH_3$, δ = 3.6 ppm, peak c) and methylene ($C–CH_2–C$, δ = 1.78 ppm, peak a), there also exists three proton signals for methyl ($–CH_3$) due to the three conformations of PMMA (isotactic, heterotactic, syndiotactic): δ= 1.27ppm for isotactic, 1.04 ppm for heterotactic, and 0.8 ppm for syndiotactic.[32] By comparing the ^{1}H NMR spectra of pure PMMA with PMMA-BFO, we can conclude that in the pure PMMA, isotactic and syndiotactic conformations are overriding while in PMMA-BFO nanocomposites, the heterotactic conformation increases, significantly.

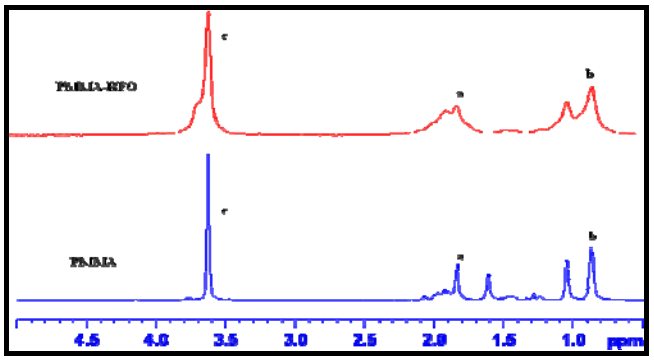

Fig. 2 ^{1}H NMR spectra of the PMMA-BFO and pure PMMA

Table 2 Tacticity of pure PMMA and PMMA-BFO nanocomposites

	% Tacticity		
	Isotactic	Heterotactic	Syndiotactic
PMMA	0.0979	0.328	0.5737
PMMA-BFO	0.068	0.38	0.54

Morphology

Fig. 3(a-d) shows the FESEM (a, b) and TEM (c, d) images of the pure BFO nanoparticles synthesized by combustion method. It can be clearly seen that the BFO nanoparticles with particle size ~ 40-60 nm are uniformly distributed throughout surface. The shapes of the nanoparticles are mostly spherical in nature while very few large particles are observed which may be due to the effect of agglomeration.

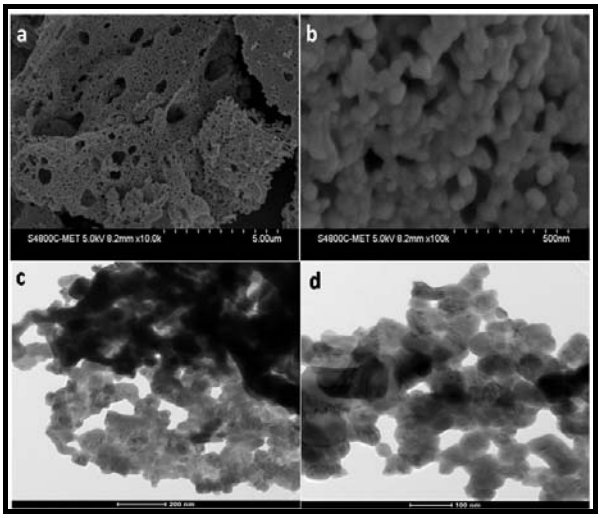

Fig.3 FESEM (a,b) and TEM (c,d) images of pure BFO

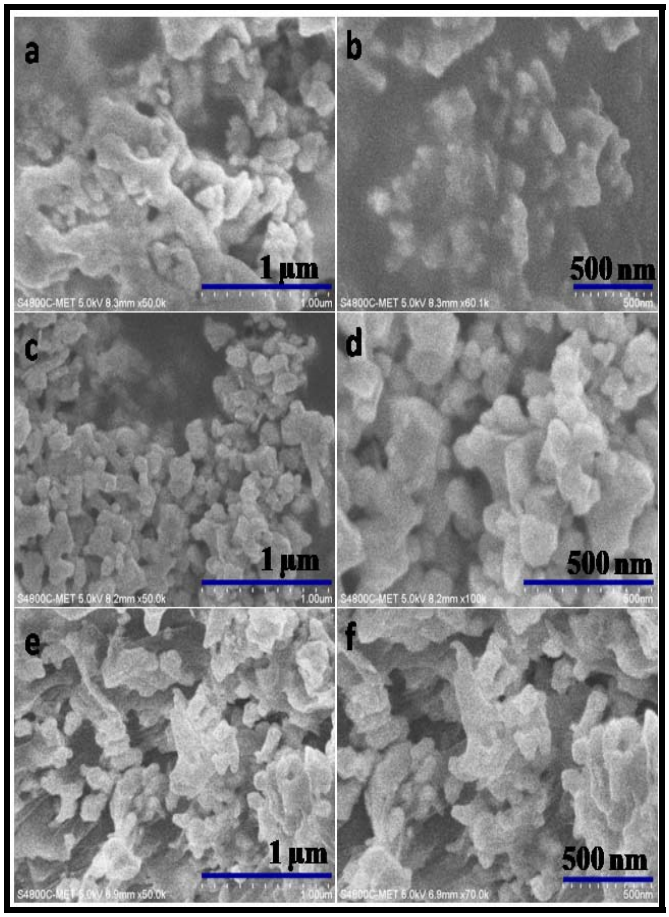

Fig. 4 (a-f) FESEM images of PMMA-BFO1 (a, b), PMMA-BFO3 (c, d) and PMMA-BFO5 (e, f) nanocomposites

Fig. 4(a, b) depicts the FE-SEM images of PMMA-BFO1 nanocomposites at low and high magnifications. The FESEM images shows that the BFO nanoparticles are merely distributed in the polymer matrix having the particle size around 20-40 nm. However, with increase in loading percentage of BFO [Fig. 4(c, d)] granular or spherical shaped particles with size ~ 40-60 nm are observed. With further increase in loading percentage of BFO, Fig. 4(e-f) uneven shaped particles (~ 60-80) nm is observed. It is quite obvious that due to agglomeration, the particle size increases with increase in BFO loading. At lower loading percentage, the dispersion of nanoparticles is fairly uniform and hence shows lower particle size as compared to pristine BFO.

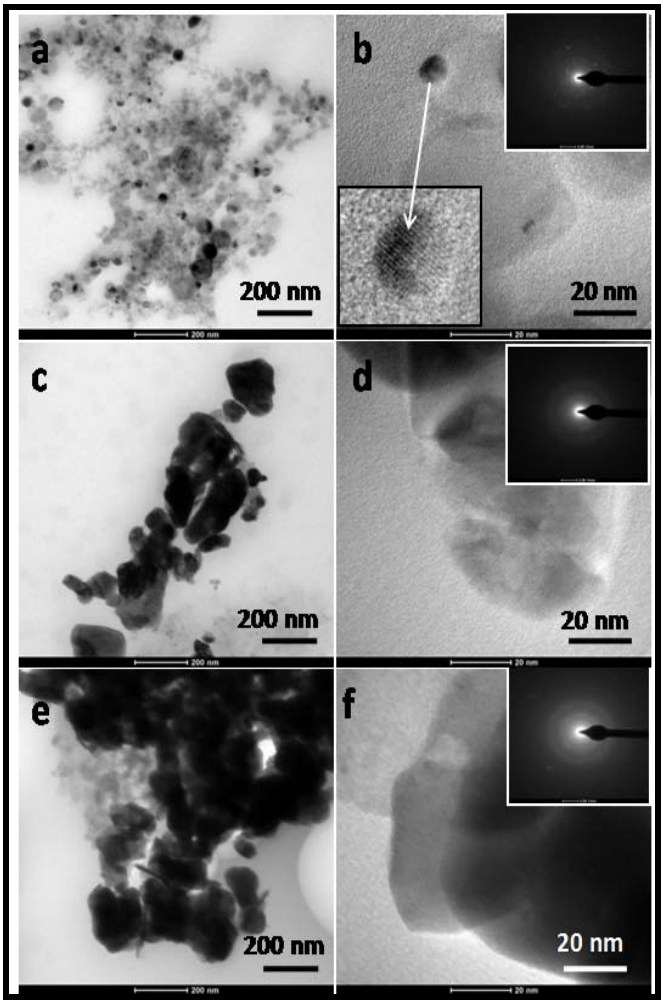

Fig. 5 TEM images of PMMA-BFO1 (a,b), PMMA-BFO3 (c,d) and PMMA-BFO5 (e,f) nanocomposites. Inset Fig. 3 (b,d,f) shows SAED pattern of PMMA-BFO nanocomposits.

Fig. 5(a-f) displays the TEM images of PMMA-BFO nanocomposites. It can be seen from Fig. 5(a-b) that at lower percentage of BFO loading, BFO nanoparticles of size 20-40 nm are uniformly distributed in the polymer matrix. From Fig. 5(c, e) it can be seen that BFO nanoparticles are embedded in the polymer matrix having particle size is found to be ~ 40-50 and 60-70 nm, respectively. The agglomeration of the particle is clearly visible at higher loading percentage (3% and 5%) of BFO. HRTEM image (Fig. 5b, d, f) have also been taken to extract more detail information about the microstructure and crystallinity of the as-prepared nanocomposites. The clear and uniform lattice fringes at lower (1%) loading percentage of BFO confirmed the enhancement in the crystalline nature of the composite (Inset in Fig.5b) which can be seen from the XRD pattern of PMMA-BFO nanocomposites. The appearance of distinctly visible rings in selected area electron diffraction (SAED) pattern at higher loading percentage of BFO confirmed the presence of

polycrystalline nature of the nanocomposites (Inset in Fig. 5b, d and f). Here also, we observed agglomeration of the particle with increase in loading percentage.

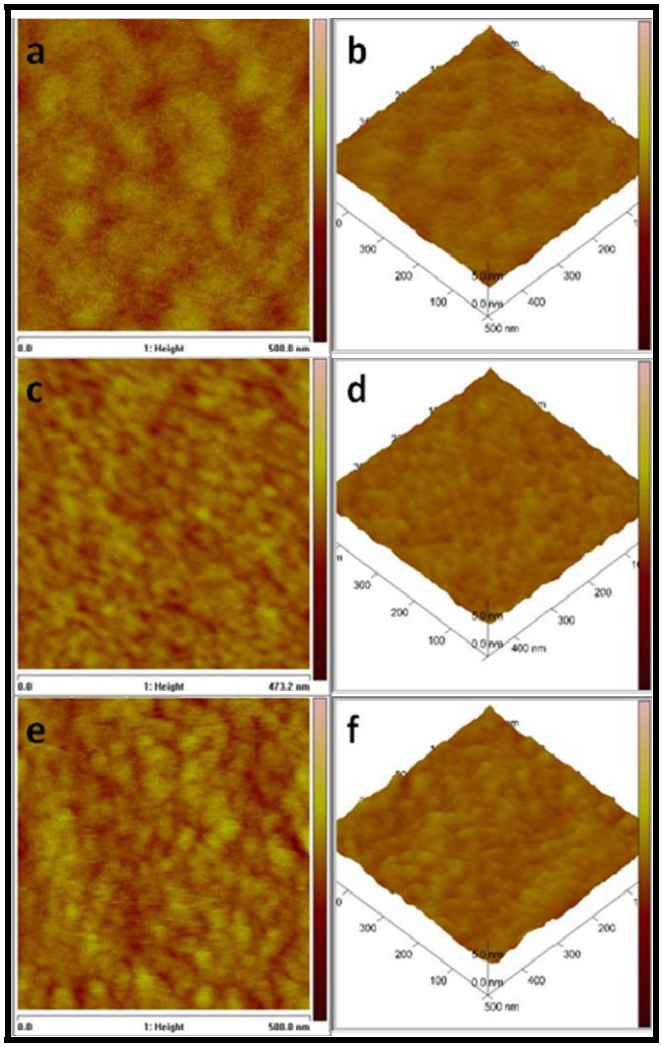

Fig. 6a, c and e show 2D (two dimensional) and Fig. 6b. d and f shows 3D (three dimensional) images of PMMA-BFO1(a,b), PMMA-BFO3 (c,d) and PMMA-BFO5 (e,f) nanocomposites

The atomic force microscopy (AFM) images of PMMA-BFO nanocomposites are shown in Fig. 6. Fig. 6 (a, c, e) and (b, d, f) shows the 2D (two dimensional) and 3D (three dimensional) images of the PMMA-BFO nanocomposites, respectively. The yellow colored spots in the 2D images of AFM represent the presence of BFO particles whereas the red colored spots represent the polymer. The surface morphology of the 2D image clearly shows that (yellow colored spots) 30-35 nm sized particles are dispersed in the PMMA matrix (red color). The 3D image also provides information about the surface roughness and the height of the BFO nanoparticles. Most of the nanoparticles have heights of around ~ 40–45 nm and there are very few particles with heights in the range of ~ 50–60 nm embedded in the PMMA matrix. The AFM images clearly show agglomeration with increase in loading percentage of BFO. The surface morphology obtained using AFM is in good agreement with the FESEM and TEM results.

Fig. 7 shows TG curves of the pure PMMA and PMMA/BFO nanocomposites. It can be seen that for pure PMMA complete degradation of polymer occurs ~ 400^{o}C but with the incorporation of BFO nanoparticle the degradation temperature was found to be slightly shifted towards the higher temperature. Additionally, to confirm the thermal stability, DSC measurements of nanocomposites have been performed. The DSC analysis clearly shows higher decomposition temperature for nanocomposites. (Supporting information Figure S1).

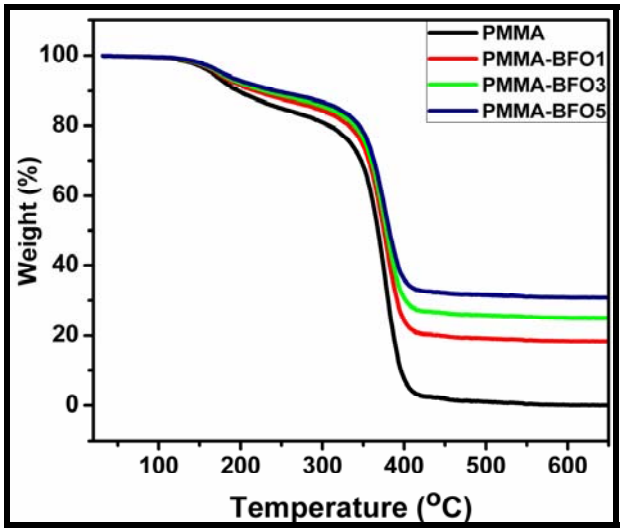

Fig. 7 TGA of Pristine PMMA, PMMA-BFO1, PMMA-BFO3 and PMMA-BFO5 nanocomposites

Reaction Mechanism

Detail formation and growth mechanism of pure BFO by combustion method is illustrated below. The combustion reaction involves an exothermic redox reaction between oxidant and fuel. Metal precursors i.e. nitrates of bismuth and iron acts as oxidizers which decompose in the presence of a fuel, provides oxygen or lose electrons. When an oxidizer and fuel are mixed in a relevant proportion, a tremendous amount of heat is generated which propagates the chemical reaction. The significant feature of this reaction is that, the amount of heat evolved during the course of reaction is more than the actual heat required for reaction. The fuel used makes complexes with the metal ions present in the precursor solution. This complex on dehydration produces a viscous gel which on further heating self ignites with the evolution of huge amount of gases. This leads to the development of porous floppy ash. Fine phase pure BFO powder can be obtained on further calcination of the ash at high temperature. The reaction mechanism for the formation of single phase BFO is shown in equation (I). Here, Glycine was used as fuel and which is capable of burning by breaking of C-H bonds or gaining electrons. The minimum temperature required for rapid reaction between oxidant and fuel is termed as ignition temperature. Sudden ignition of oxidant - fuel mixture completes within short time and makes chemical reaction self sustaining which in turn an advantage of this process over others. During the auto combustion process lots of fumes are generated which may be due to evolution of several gases like NO_2, CO_2, CH_4, NH_3 and H_2O which is shown in equation I. Initially, all these gases get evolved and form BFO nuclei or very small nanoparticles. Then further calcination at 500 ^{0}C, accelerate the crystal growth of

nuclei or small nanoparticles. The smaller crystals get agglomerated and form bigger crystals during the calcination. It is quit understood that the crystal growth of BFO is taking place as per the well known phenomena Ostwald ripening. [52]

$$Bi(NO_3)_3.5H_2O + Fe(NO_3)_3.9H_2O + NH_2CH_2COOH \xrightarrow{500^0C} BiFeO_3 + 6NO_2 + nH_2O + NH_3 \uparrow + CH_4 \uparrow + CO_2 \uparrow \quad \text{... (I)}$$

Scheme 1: The reaction mechanism of BFO formation

Scheme 2 presents the general process to synthesize the PMMA-BFO nanocomposites. In the schematic representation, it can be seen that the monomer (MMA) is wrapped on the BFO nanoparticles during the polymerization reaction. The further polymerization of MMA (coated on BFO) gives PMMA wrapped on BFO (PMMA-BFO) using oxidizing agent BPO. Agglomeration of the particle is observed in the nanocomposites due to increase in the loading percentage of BFO.

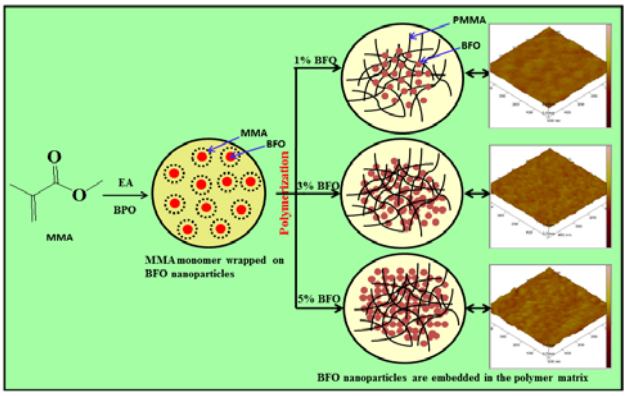

Scheme 2: Formation mechanism of PMMA-BFO nanocomposites

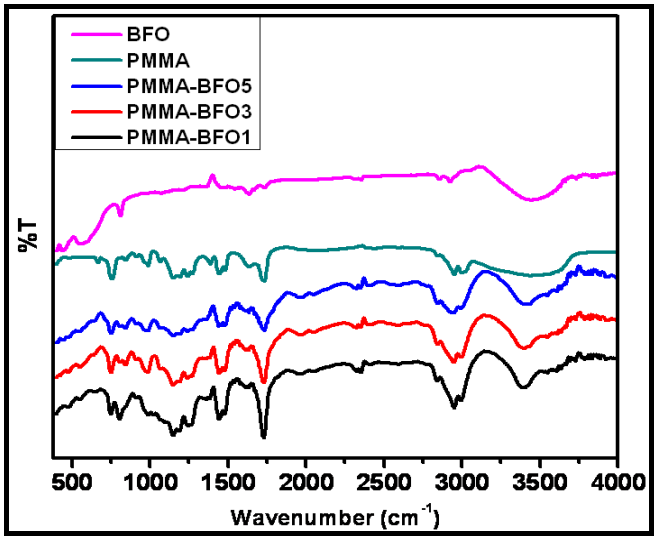

Fig. 8 FTIR Spectra of Pristine PMMA, BFO and PMMA-BFO1, PMMA-BFO3 and PMMA-BFO5 nanocomposites

FTIR Spectra

The FTIR spectrum of Pristine PMMA, BFO and PMMA-BFO1, PMMA-BFO3 and PMMA-BFO5 nanocomposites are shown in Fig.8. It is evident here that for pure BFO the presence of broad band at ~3000–3600 cm^{-1} arose from the asymmetric and symmetric stretching of OH^- groups, while a band at 1630 cm^{-1} corresponds to the bending vibrations of H_2O molecule [53, 54] Particularly, two strong absorption peaks around 549.75 and 439.80 cm^{-1} are attributed to the Fe-O stretching and O-Fe-O bending vibrations, being characteristics of the octahedral FeO_6 groups in the perovskite compounds. The presence of metal-oxygen band confirmed the development of perovskite structure in BFO. [55]Fig. 8 shows the details of functional groups present in the pristine PMMA. A sharp intense peak appeared at 1872 cm^{-1} is due to the presence of ester carbonyl group stretching vibration, C=O stretching. [56]The broad peak ranging from 1260-1000 cm^{-1} can be explained owing by the C-O (ester bond) stretching vibration. The broad peak ranging from 2900-4000 cm^{-1} is attributed to the presence of stretching vibration and a peak at 1195 cm^{-1} is assigned to –O-CH3 stretching vibrations.[57] Similarly, figure 8 spectra shows the FTIR spectra of PMMA-BFO1,PMMA-BFO3 and PMMA-BFO5 nanocomposites respectively. The comparison of the FTIR spectra between the pure BFO, PMMA and PMMA-BFO (1, 3 and 5%) nanocomposites shows both peaks of BFO and PMMA.

Dielectric Measurement

The frequency dependence of room temperature dielectric constant and dielectric loss of the PMMA-BFO nanocomposites are shown in Fig. 9 (a & b). It can be seen that the dielectric constant of the nanocomposites increases with increasing BFO content over the whole frequency range. A much higher increase of dielectric constant can be observed at the higher BFO content. For instance, at 1 kHz, the dielectric constant is ~ 6.9 for PMMA-BFO1 ($BiFeO_3$ concentration is about 1 %) and ~ 14 for PMMA-BFO5 ($BiFeO_3$ concentration is about 5 %). It can also be observed that the value of dielectric constant decreases with increase in frequency. The decreasing behavior of dielectric constant with the increase in frequency can be explained on the basis of dispersion of polarization with frequency. Dielectric polarization in a material is the sum total of the different polarization mechanisms; such as electronic, ionic, dipolar and interfacial polarization. The mechanisms of polarization have varying time response dependence on the frequency of the applied field and the net contribution of polarization to the dielectric constant is therefore frequency dependent. At lower frequency all the polarizations respond easily to the time varying electric field but as the frequency of the field increases different polarizations are filtered out. Hence, the overall polarizations of the material decreases which leads to the decrease in the value of dielectric constant.

It can also be seen that the nanocomposites show inherent low loss over a wide range of frequencies (10 Hz to 1 MHz). The dielectric loss of the nanocomposites decreases with the increase in frequency (Fig. 9 b). However, there is an increment in dielectric loss is observed after the 100 kHz frequency, which may be due to the relaxation mechanism present in the polymer. The higher value of tanδ at low frequency can be attributed due to the relaxation of the space charge polarization. The further increase of tanδ with the increase in frequency in the samples may be due to relaxation of the domain wall pinned at defects in the crystal. [58, 59]

Dielectric loss of the nanocomposite is found to be slightly higher than the polymer matrix. These features were consistent

with the dielectric loss result reported in the literature, which may be due to the relatively high dielectric loss of the BFO nanoparticles loading. Considering that the nanocomposites have a significantly increased dielectric constant and comparable dielectric loss, we can say that in situ ATRP could be a promising method to fabricate dielectric materials for high dielectric constant films. Fig. 10 also presents the frequency dependence of ac electrical conductivity of the nanocomposites. The ac electrical conductivity of the composites increases with the increase in frequency for all the samples and is only slightly higher than that of pure PMMA over the whole frequency range, indicating the good insulating properties of the nanocomposites. The observed low electrical conductivity of the composites in comparison to the pure BFO samples is due to the fact that BFO nanoparticles are capped by insulating polymer shells and show homogeneous dispersion in the polymer matrix, which prevent electron conduction resulting in the lower leakage current and lower dielectric loss of the nanocomposites.

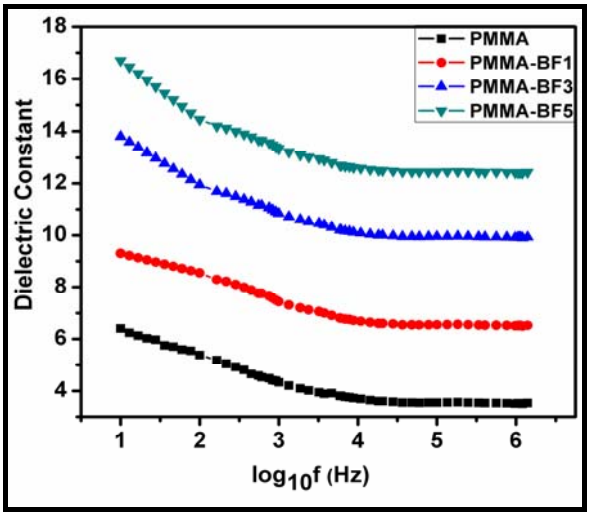

Fig. 9 (a) Frequency dependence of dielectric constant of PMMA, PMMA-BFO1, PMMA-BFO3 and PMMA-BFO5 nanocomposites at room temperature

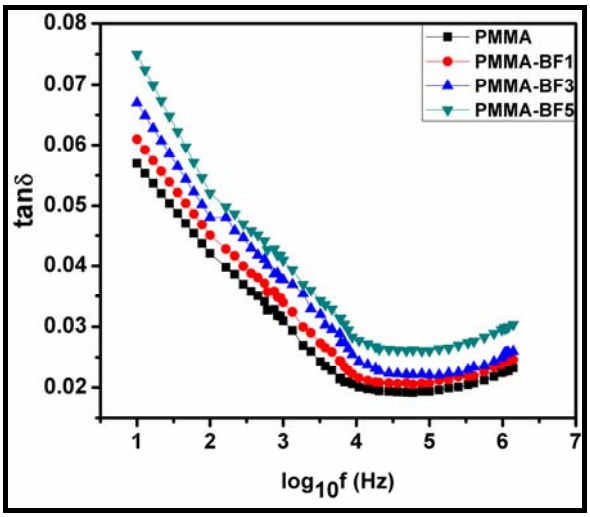

Fig. 9 (b) Frequency dependence of dielectric loss of PMMA, PMMA-BFO1, PMMA-BFO3 and PMMA-BFO5 nanocomposites at room temperature

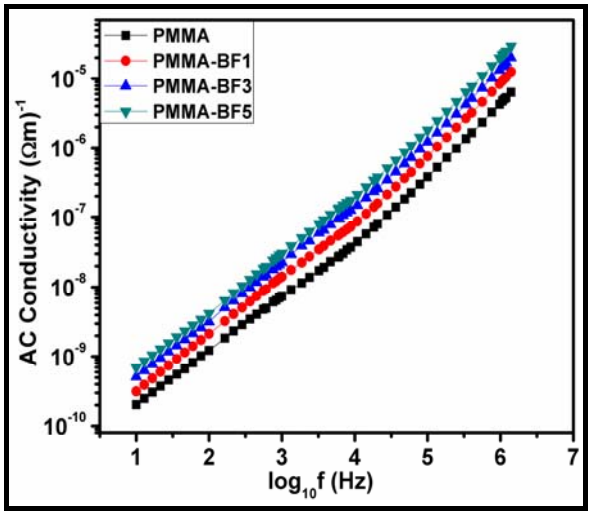

Fig. 10 Frequency dependence of ac electrical conductivity of PMMA, PMMA-BFO1, PMMA-BFO3 and PMMA-BFO5 nanocomposites at room temperature

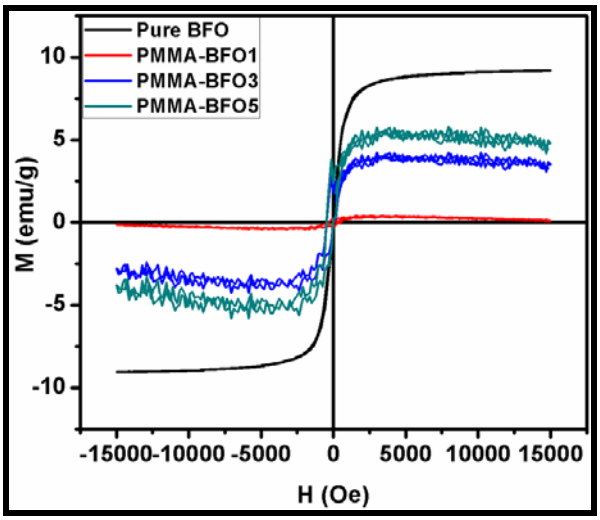

Fig.11 M-H loops of the BFO, PMMA-BFO1, PMMA-BFO3 and PMMA-BFO5 nanocomposites at room temperature

Fig.11 shows the room temperature Magnetic hysteresis loop of the pure BFO as well as PMMA-BFO nanocomposites. The development of well saturated M-H loop confirms the ferromagnetic nature of all the samples. The value of saturation magnetization (M_s) as well as remnant magnetization (M_r) of pure BFO sample is found to be higher than the nanocomposites. It can also be seen that with the increase in loading percentage of BFO powder in the composite, the value of M_s and M_r increases linearly which may be due to the increase in magnetic particles in the nanocomposites. The value of saturation magnetization in case of 1% BFO filled polymer composite was found to be ~ 0.4 emu/g whereas the value of M_s for 5% was found to be ~ 6 emu/g, which is due to the increase of loading percentage of magnetic nanoparticles.

The increase of M_s value with the increase in loading percentage of BFO nanoparticles can be explained by the following equation:

$$Ms = \phi m_s \quad \text{..... (II)}$$

Where M_s is related to the percentage of BFO nanoparticles (ϕ) and the saturation moment of a single particle (m_s). In all the nanocomposite samples, a very small value of coercive field (H_c) is observed, which indicates that the material can be useful for memory applications.

The result obtained in this study has been compared with the previously reported results and is given in Table-2. It can be seen that our results are far better than the reported results.

Table-2 Comparison between the dielectric and magnetic properties of PMMA-BFO5 with the reported results

Sample Name	Dielectric constant (10 kHz)	Dielectric loss (10 kHz)	Saturation Magnetization	Reference Number
10% v BFO +PMMA	~ 6.5	~ 0.005	1 emu/cc3	50
BaTiO3–PMMA (15 v% BaTiO3)	~ 6.2	~0.035	----------	30
5 wt% BFO + PMMA	~ 13.6	~ 0.03	6 emu/g	Present work

Conclusions

Poly (methyl methacrylate) PMMA-BFO nanocomposites were successfully synthesized by *in-situ* polymerization method. XRD results confirm the formation of single phase BFO ceramics. The presence of both BFO and PMMA peaks in the nanocomposite indicated the development of both polymer as well as ceramic phases. The agglomeration of the particles were found to increase with the increase of the loading percentage of BFO particles which is supported by field emission-scanning electron microscopy (FE-SEM), transmission electron microscopy (TEM) and atomic force microscopy (AFM) images. The FTIR spectra confirm the complexation and interaction among the compounds. The interaction influences the structural interphase changes in the PMMA-BFO nanocomposites. ^{1}H NMR shows the confirmation of PMMA and PMMA-BFO group in the nanocomposites. A broadband dielectric spectroscopy was used to investigate the dielectric properties of the nanocomposites in a frequency range from 10 Hz to 1 MHz. It was found that the value of dielectric constant was significantly increased with increase in loading percentage of BFO as compared to pure PMMA. It also showed inherent low dielectric loss in a wide range of frequencies. Development of well saturated magnetic hysteresis loop confirmed the ferromagnetic nature of the BFO ceramics. The ferromagnetic nature was also retained in the PMMA-BFO nanocomposites. The value of M_s of the PMMA-BFO nanocomposite was increased with the increase in BFO content. The dielectric results in this study indicated that the nanocomposites can be a potential candidate for high dielectric constant capacitor applications. Whereas, the magnetic properties suggested that the nanocomposite can be useful for electromagnetic applications like electromagnetic interference suppressor in the frequency as well as hard disc components.

Acknowledgement

Authors are thankful to Dr. D. P. Amalnerkar, Executive Director, C-MET, for his constant encouragement. Authors also would like to thank DIT, New Delhi, for financial support. Authors are thankful to Nanocrystalline group for their generous help.

Notes and references

[a] *Nanocomposite Laboratory, Centre for Material for Electronics Technology (C-MET), Department of Information Technology, Govt. of India, Panchawati, off Pashan Road, Pune 411 007, INDIA. Fax: +91 20 2589 8180; Tel: +91 20 2589 9273;*
E-mail: kbbb1@yahoo.com, bbkale@cmet.gov.in
[b] *School of Chemical Sciences, Solapur University Solapur - 411255*

References

1. J. P Dhal and S. C. Mishra, Journal of Polymer Composites, 2013, 1, 28-32.
2. A. Patsidis and G. C. Psarras, EXPRESS Polymer Letters, 2008, 2, 718–726.
3. J. R. Yoon, J.W. Han and K. M. Lee and H. Y. Lee, Transactions of Electrical and Electronic Materials 2009, 10, 1229-7607
4. M. Arbatti, X. B. Shan and Z. Y. Cheng, Adv. Mater., 2007, 19, 1369–1372.
5. Z. M. Dang, Y. H. Lin and C. W. Nan, Adv. Mater., 2003, 15, 1625.
6. L. Qi, B. I. Lee, S. H. Chen, W. D. Samuels and G. J. Exarhos, Adv. Mater., 2005, 17, 1777–1781.
7. N. Guo, S. DiBenedetto, D. Kwon, L. Wang, M. Russell, M. Lanagan, A. Facchetti and T. Marks, J. Am. Chem. Soc., 2007, 129, 766–767.
8. J. Yao, C. Xiong, L. Dong, Y. Lei, L. Chen, R. Li, Q. Zhu and X. Liu, J. Mater.Chem. 2009, 19, 2817–2821.
9. M. N. Tchoul, S. P. Fillery, H. Koerner, L. F. Drummy, F. T. Oyerokun, P. A. Mirau, M. F. Durstock and R. A. Vaia, Chem. Mater., 2010, 22, 1749–1759.
10. X. Y. Huang, L. Y. Xie, P. K. Jiang, G. L. Wang and F. Liu, J. Phys. D: Appl. Phys., 2009, 42, 245407.
11. K. Brandt, C. Neusel, S. Behr and G. Schneider, J. Mater. Chem. C, 2013,1, 3129-3137.
12. M. Rahimabady, M. Mirshekarloo, K. Yao and L. Lu, Phys. Chem. Chem. Phys., 2013,15, 16242-16248.
13. Y. Bai, Z. Y. Cheng, V. Bharti, H. S. Xu and Q. M. Zhang, Appl. Phys. Lett., 2000, 76, 3804–3806.
14. G. Sarasqueta, K. R. Choudhury, D. Y. Kim and F. So, Appl. Phys. Lett., 2008, 93, 123305.
15. J. Yuan, Z. Dang, S. Yao, J. Zha, T. Zhou, S. Li and J. Bai, J. Mater. Chem., 2010, 20, 2441–2447.
16. H. Xu, Z. Dang, M. Jiang, S. Yao and J. Bai, J. Mater. Chem., 2008, 18, 229–234.
17. Y. Rao, S. Ogitani, P. Kohl and C. P. Wong, J. Appl. Polym. Sci., 2002, 83, 1084– 1090.
18. Y. Rao and C. P. Wong, J. Appl. Polym. Sci., 2004, 92, 2228–2231.
19. Q. M. Zhang, H. F. Li, M. Poh, F. Xia, Z. Y. Cheng, H. S. Xu and C. Huang, Nature, 2002, 419, 284–287.
20. Y. Deng, Y. Zhang, Y. Xiang, G. Wang and H. Xu, J. Mater. Chem., 2009, 19, 2058–2061.
21. J. Lu, K. Moon and C. Wong, J. Mater. Chem., 2008, 18, 4821–4826.
22. Z. Dang, L.Wang, Y. Yin and Q.Zhang, Adv.Mater., 2007, 19, 852–857.
23. X. Y. Huang, P. K. Jiang and L. Y. Xie, Appl. Phys. Lett., 2009, 95, 242901.
24. J. W. Xu and C. P. Wong, Appl. Phys. Lett., 2005, 87, 082907.
25. J. X. Lu, K. S. Moon, J. W. Xu and C. P. Wong, J. Mater. Chem., 2006, 16, 1543-1548.
26. X. Y. Huang, C. U. Kim, P. K. Jiang, Y. Yin and Z. Li, J. Appl. Phys., 2009, 105, 014105.
27. K. Han, Q. Li, Z. Chen, M. R. Gadinski, L. Dong, C. Xiong and Q. Wang, J. Mater. Chem. C, 2013,1, 7034-7042.
28. D. Wang, T. Zhou, J. Zha, J. Zhao, C. Shi and Z. Dang, J. Mater. Chem. A, 2013,1, 6162-6168.
29. Y. Shen, Y. H. Lin and C. W. Nan, Adv. Funct. Mater., 2007, 17,

2405–2410.
30. L. Xie, X. Huang, C. Wu and P. Jiang, J. Mater. Chem., 2011, 21, 5897-5906.
31. D. Bhadra, A. Biswas, S. Sarkar, B. K. Chaudhuri, K. F. Tseng and H. D. Yang, J. Appl. Phys., 2010, 107, 124115.
32. R. E. Newnham. Composite Electroceramics. Annu. Rev.Mater.Sci. 1986, 16: 47- 68.
33. D. K. Das-Gupta. Ferroelectric polymer and ceramic-polymer composites. Tran. Tech. Aedermannsdorf, Switzerland 1994.
34. C. J. Dias and D. K. Das-Gupta, Trans.Dielectr Electr Insul 1996, 3, 706.
35. D. H, Kuo, C. C. Chang, T.Y. Su, W. K. Wang and B. Y. Lin, J.Eur.Ceram Soc., 2001, 21, 1171.
36. H. Zewdie and F. Brouers. J.Appl.Phys. 1990, 68, 713.
37. T. Yamada, T. Ueda and T. Kitayama. J.Appl.Phys, 1982, 53, 4328
38. J. B. Ngoma, J. Y. Cavaille, J. Paletto, J. Perez, F. Macchi. Ferroelectrics 1990, 109, 205-210.
39. M. J. Abdullah and D. K. Das-Gupta. Ferroelectrics, 1987, 76, 393-401.
40. M. J. Abdullah and D. K. Das-Gupta. Proc.6th International Symposium on Electrets, Oxford, IEEE Service Centre, Piscaraway 1988
41. D. K. Das-Gupta and M. J. Abdullah. J.Mater.Sci.Lett,1988, 7, 167-170.
42. Y. Daben. Feroelectrics, 1990, 101, 291.
43. L.A. Ramajo, A.A. Cristobal, P.M. Botta, J.M. Porto Lopez, M.M. Reboredo and M.S. Castro, Composites Part A 2009, 40, 388–393.
44. A.S. Bhatt, D. Krishna and M.S. Santosh, Journal of Applied Polymer Science, 2011,119, 968–972.
45. C. Kim, K.S. Yang, Appl. Phys. Lett. 2006, 83, 1216.
46. Z.Y. Li, H.N. Zhang, W. Zheng, J. Am. Chem. Soc. 2008, 130, 5036.
47. J. Wang, J. B. Neaton, H. Zheng, V. Nagarajan, S. B. Ogale, B. Liu, D. Viehland,V. Vaithyanathan, D. G. Schlom, U. V. Waghmare, N. A. Spaldin, K. Rabe, M. Wuttig and R. Ramesh, Science 2003, 299, 1719.
48. R. Palai, R. S. Katiyar, H. Schmid, P. Tissot, S. J. Clark, J. Robertson, S. A. T. Redfern, G. Catalan and J. F. Scott, Phys. ReV. B 2008, 77, 014110.
49. Y. H. Lin, Q. Jiang, Y. Wang, C. W. Nan, L. Chen, J. Yu, Appl. Phys. Lett. 2007, 90, 172507.
50. A. Ahlawat, S. Satapathy, S. Bhartiya, M. K. Singh, R. J. Choudhary, Appl. Phys. Lett., 2014, (DOI:10.1063/1.4863228)
51. W. H. Sun, D. S. Hung, T. T. Song , Y. P. Fu, and S. F. Lee, IEEE TRANS MAGN 2011, 47, 4306-4309
52. Y. Liu, K. Kathan, W. Saad and R. K. Prud'homme Physical Review Letter, 2007, **98,** 036102.
53. A.Z. Simo˜es, B.D. Stojanovic, M.A. Ramirez, A.A. Cavalheiro, E. Longo and J.A.Varela, Ceram. Int. 2008, 34, 257.
54. Z.V. Gabbasova, M.D. Kuz'min, A.K. Zvezdin, I.S. Dubenko, V.A. Murashov, D.N. Rakov and I.B. Krynetsky, Phys. Lett. A. 1991, 158, 491.
55. W. Luo, L. Zhu, N. Wang, H. Tang, M. Cao and Y. She, Environ. Sci. Technol. 2010, 44, 1786-1791.
56. N. Singh and P.K. Khanna, Mater. Chem. And Phys. 2007, 104, 367-372.
57. A. Balamurugan, S. Kannan, V. Selvaraj and S.Rajeswara, Artif. Organs 2004, 18, 41-45.
58. G. Luther, phys status solidi (a), 1973, 20, 227–236.
59. P. Kumar and P. Palei, Integr Ferroelectr, 2010,121, 24-30.

Table of Content

Polymethyl methacrylate (PMMA) –Bismuth Ferrite (BFO) nanocomposite: Low loss and high dielectric constant materials with perceptible magnetic properties

Mohaseen S. Tamboli, Prakash K. Palei, Santosh S. Patil, Milind V. Kulkarni, Noormahmad. N. Maldar and Bharat B. Kale

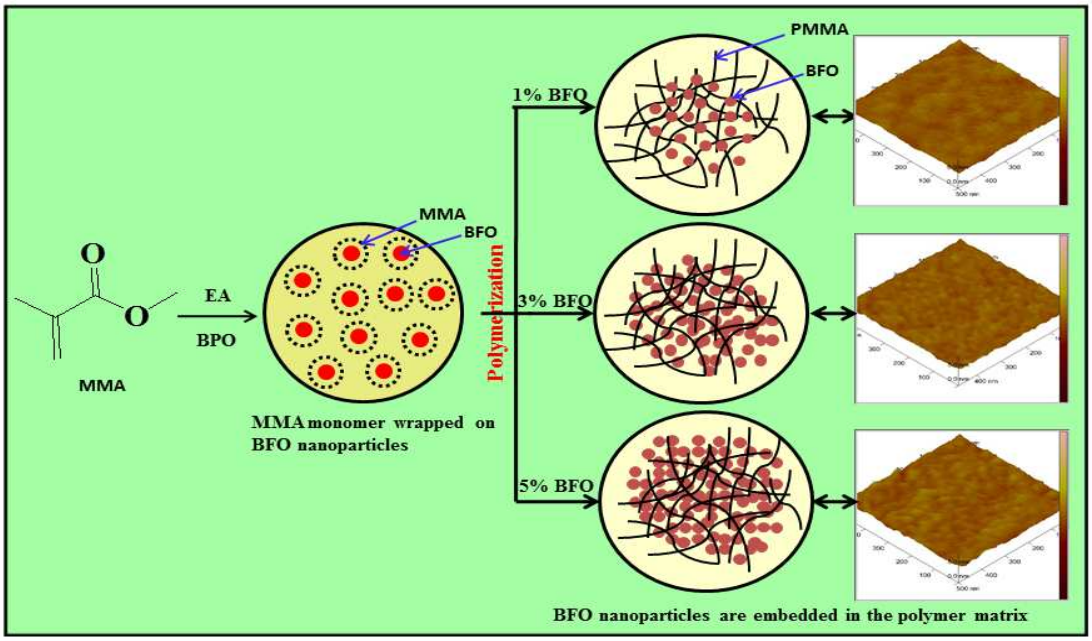

Formation mechanism of PMMA-BFO nanocomposites